EDGE ARTICLE

Wide band gap selenide infrared nonlinear optical materials $A^{II}Mg_6Ga_6Se_{16}$ with strong SHG responses and high laser-induced damage thresholds†

Linan Wang,‡[ab] Dongdong Chu,‡[ab] Zhihua Yang, [ab] Junjie Li [*ab] and Shilie Pan [*ab]

Infrared (IR) nonlinear optical (NLO) materials with strong NLO response, wide band gap and high laser-induced damage threshold (LIDT) are highly expected in current laser technologies. Herein, by introducing double alkaline-earth metal (AEM) atoms, three wide band gap selenide IR NLO materials $A^{II}Mg_6Ga_6Se_{16}$ (A^{II} = Ca, Sr, Ba) with excellent linear and NLO optical properties have been rationally designed and fabricated. $A^{II}Mg_6Ga_6Se_{16}$ (A^{II} = Ca, Sr, Ba) are composed of unique $[A^{II}Se_6]$ triangular prisms, $[MgSe_6]$ octahedra and $[GaSe_4]$ tetrahedra. The introduction of double AEMs effectively broadens the band gaps of selenide-based IR NLO materials. Among them, $CaMg_6Ga_6Se_{16}$, achieving the best balance between the second-harmonic generation response ($\sim$1.5 × $AgGaS_2$), wide band gap (2.71 eV), high LIDT ($\sim$9 × $AgGaS_2$), and moderate birefringence of 0.052 @ 1064 nm, is a promising NLO candidate for high power IR laser. Theoretical calculations indicate that the NLO responses and band gaps among the three compounds are mainly determined by the NLO-active $[GaSe_4]$ units. The results enrich the chemical diversity of chalcogenides, and give some insight into the design of new functional materials based on the rare $[A^{II}Se_6]$ prismatic units.

Introduction

Nonlinear optical (NLO) crystals are an important class of optoelectronic functional materials, which play a critical role in developing new laser light sources by the frequency conversion technology.[1–8] In the ultraviolet (UV) and visible-near infrared (IR) regions, oxide-based NLO materials have achieved great progress,[9–13] and a series of NLO crystals with excellent performances like LiB_3O_5 (LBO), BaB_2O_4 (β-BBO), $KBe_2BO_3F_2$ (KBBF), KH_2PO_4 (KDP), and $NH_4B_4O_6F$ have been developed in recent years,[14–18] while in the mid- and far-IR regions, the commercially available IR NLO materials like $AgGaS_2$ (AGS), $AgGaSe_2$ (AGSe) and $ZnGeP_2$ (ZGP) suffer from their intrinsic defects, like low laser-induced damage thresholds (LIDTs) in AGS and AGSe, strong two-photon absorption around $\sim$1 μm and narrow IR transparent range in ZGP.[19,20] Therefore, exploring new IR NLO

materials with excellent performances has become an urgent need, but challenging due to the conflicts among NLO response, band gap, birefringence and IR transparent range in one material.[21]

For an excellent IR NLO material, the following requirements should be satisfied:[22] (1) noncentrosymmetric (NCS) crystal structure; (2) a large NLO response ($\geq$0.5 × AGS, preferably $\geq$1.0 × AGS); (3) a wide IR transparent range that covers the two important IR atmospheric windows of 3–5 and 8–12 μm; (4) a high LIDT, which is usually related to the band gap and thermal conductivity; (5) suitable birefringence for phase-matching (PM) behavior; (6) good crystal growth habits. To achieve the large NLO response and wide IR transparent range, metal selenide has been demonstrated as a competitive system, due to the large hyperpolarizability of NLO-active $[MSe_4]$ (M = Ga, In, Ge, Sn, Zn, Cd, Hg, *etc.*) tetrahedral units, and red shift of the vibration peaks of M–Se compared to M–O, M–S or M–P bonding.[23,24] However, for most selenides, their band gaps are narrow due to the presence of outer electrons on the 3d, 4s, 4p orbits in the Se atom.[25,26]

To enhance the band gap of chalcogenides, introducing an alkaline-earth metal (AEM) without d–d and f–f electron transitions into the crystal structures has been regarded as a feasible strategy.[27,28] Recently, by coupling $[MgQ_6]$ (Q = S, Se) octahedral and $[MQ_4]$ (M = Al, Ga) tetrahedral units, a series of Mg-containing compounds $A^IB_3^{II}C_3^{III}Q_8^{VI}$ (A^I = Li, Na, Ag; B^{II} = Mg; C^{III} = Al, Ga; Q^{VI} = S, Se) have been developed.[29] In this

aResearch Center for Crystal Materials, State Key Laboratory of Functional Materials and Devices for Special Environmental Conditions, Xinjiang Key Laboratory of Functional Crystal Materials, Xinjiang Technical Institute of Physics & Chemistry, CAS, 40-1 South Beijing Road, Urumqi 830011, China. E-mail: lijunjie@ms.xjb.ac.cn; slpan@ms.xjb.ac.cn

bCenter of Materials Science and Optoelectronics Engineering, University of Chinese Academy of Sciences, Beijing 100049, China

‡ L. A. Wang and D. D. Chu contributed equally to this work.

work, by introducing double AEM atoms, three wide band gap selenide IR NLO materials $A^{II}Mg_6Ga_6Se_{16}$ (A^{II} = Ca, Sr, Ba) have been synthesized by the high temperature solid-state reactions in sealed quartz tubes. $A^{II}Mg_6Ga_6Se_{16}$ (A^{II} = Ca, Sr, Ba) crystallize in the NCS $P\bar{6}$ space group, and are built by $[A^{II}Se_6]$ triangular prisms, $[MgSe_6]$ octahedral and $[GaSe_4]$ tetrahedral units. The compounds show balanced optical properties including strong second-harmonic generation (SHG) responses (1.5 × AGS for $CaMg_6Ga_6Se_{16}$, 1.0 × AGS for $SrMg_6Ga_6Se_{16}$, 1.1 × AGS for $BaMg_6Ga_6Se_{16}$), wide band gaps (in selenides) (2.69–2.71 eV), high LIDTs (8.0–9.0 × AGS), and moderate birefringences (0.044–0.052 @ 1064 nm). Density functional theory (DFT) calculations reveal that the SHG responses and band gaps of the compounds are mainly determined by the $[GaSe_4]$ tetrahedral units.

Results and discussion

The single crystals of $A^{II}Mg_6Ga_6Se_{16}$ (A^{II} = Ca, Sr, Ba) were synthesized by high temperature solid-state reactions at 900 °C, and were picked under an optical microscope for structural determinations by single crystal X-ray diffractions. The energy dispersive X-ray spectroscopy (EDS) spectra and elemental maps demonstrate the presence of Ca/Sr/Ba, Mg, Ga, Se in the structures (Fig. S1†). Meanwhile, the Raman spectra confirm the chemical bonding in the compounds (Fig. S2†). The calculated

bond valence sums and global instability indexes (Tables S2, S6 and S10†) verify the reasonability of the crystal structures in the compounds. The crystal data and structure refinement information including atomic coordinates and equivalent isotropic displacement parameters, bond length and angle information are provided in Tables S1–S13.†

Since the three compounds show similar cell parameters and crystal structures, $CaMg_6Ga_6Se_{16}$ is utilized as an example to illustrate their structures here. $CaMg_6Ga_6Se_{16}$ crystallizes in the $P\bar{6}$ space group with $a = b = 17.5327(3)$ Å, $c = 7.7603(2)$ Å. In the asymmetric unit of $CaMg_6Ga_6Se_{16}$, there are three Ca atoms, six Mg atoms, three Ga atoms and eleven Se atoms. The Ca atom and Mg atom are coordinated with Se atoms to form $[CaSe_6]$ triangular prisms and $[MgSe_6]$ octahedral units, while Ga atoms are bonded to four Se atoms to construct $[GaSe_4]$ tetrahedra (Fig. 1a). $[GaSe_4]$ tetrahedra are connected with each other by vertex-sharing to form the $[GaSe_3]$ single-chains and $[Ga_2Se_5]$ double-chains (Fig. 1a). $[MgSe_6]$ octahedra are linked with each other by edge-sharing to form $[MgSe_4]$ single-chains and $[Mg_2Se_6]$ double-chains (Fig. 1b). The formed $[GaSe_3]$ and $[MgSe_4]$ single-chains are linked by vertex-sharing to build the windmill-like $[Mg_3Ga_3Se_{24}]$ channels (Fig. 1c), which are further grouped with $[Ga_2Se_5]$ and $[Mg_2Se_6]$ double-chains to form the channel-like $[Mg_9Ga_9Se_{24}]$ framework (Fig. 1d). The six-coordinated Ca ions are filled in the channels (Fig. 1e) to balance the charge, resulting in the final 3D structure of
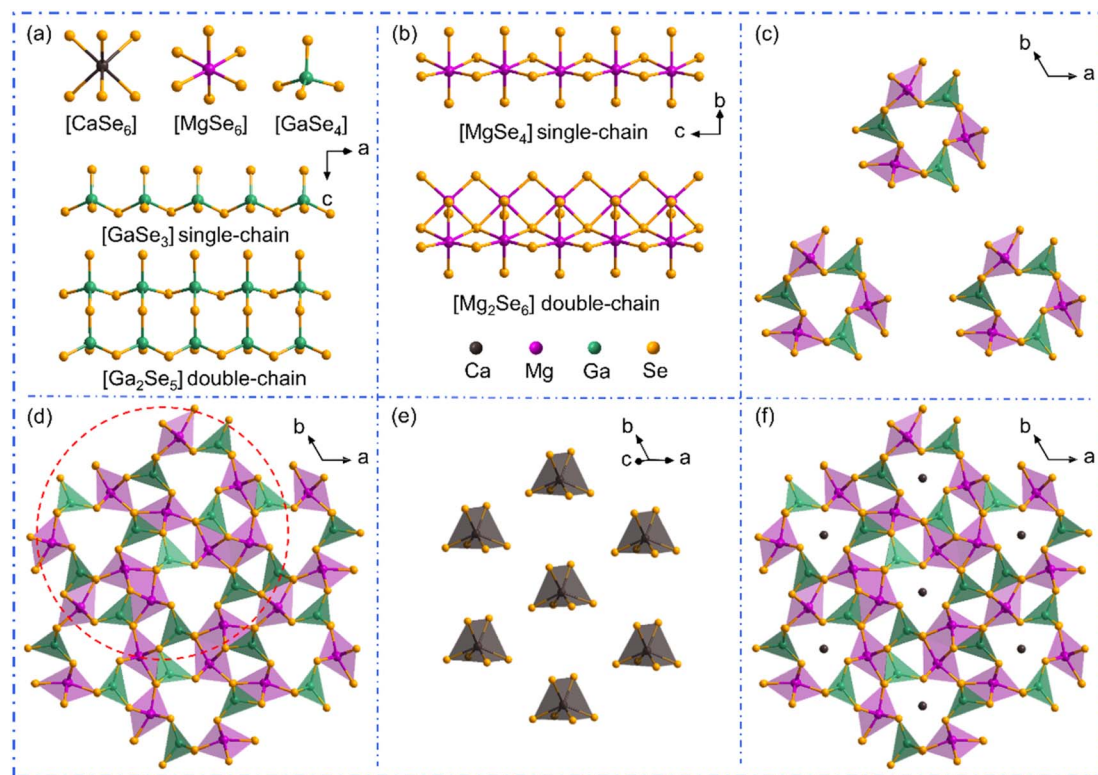

Fig. 1 The crystal structure of $CaMg_6Ga_6Se_{16}$. (a) The coordination environment of Ca, Mg and Ga atoms, $[GaSe_3]$ single-chain and $[Ga_2Se_5]$ double-chain viewed from the b direction; (b) $[MgSe_4]$ single-chain and $[Mg_2Se_6]$ double-chain viewed from the a direction; (c) windmill-like $[Mg_3Ga_3Se_{24}]$ geometries; (d) $[Mg_9Ga_9Se_{24}]$ framework; (e) $[CaSe_6]$ triangular prisms; (f) the 3D structure of $CaMg_6Ga_6Se_{16}$ viewed from the c direction.

$CaMg_6Ga_6Se_{16}$ (Fig. 1f). It is worth noting that, different from $CaMg_6Ga_6Se_{16}$ and $SrMg_6Ga_6Se_{16}$, the asymmetric unit of $BaMg_6Ga_6Se_{16}$ contains two crystallographically independent Ba atoms at Wyckoff $1c$, $1e$ positions, and two partially occupied Ba atoms with the site occupancy of 0.9 and 0.1 at Wyckoff $1a$, $1b$ positions, respectively.

Compared to the crystal structures of $A^IB^{II}_3C^{III}_3Q^{VI}$ family compounds, the title compounds can be regarded as the atomic aliovalent substitution of monovalent A^I (A^I = Li, Na, Ag) by divalent AEM A^{II} (A^{II} = Ca, Sr, Ba). The aliovalent substitution does not cause the change of space group, but induces a doubled cell parameter c in $A^{II}Mg_6Ga_6Se_{16}$ compared to $A^IMg_3Ga_3Se_8$, which can be attributed to the formed ordered vacancy in $A^{II}Mg_6Ga_6Se_{16}$ (A^{II} = Ca, Sr), or the partially occupied Ba atoms in $BaMg_6Ga_6Se_{16}$. In addition, accompanying the fluctuation of A-site cations (Fig. 2a), the channel size fluctuates from 2.49–2.56 Å to 2.39–2.65 Å (Fig. 2b). Most of them are smaller than the A^I/A^{II}–Se bond lengths in the compounds, except in the case of $AgMg_3Ga_3Se_8$ (Fig. 2b). It is worth noting that Ag is three-coordinated with three Se atoms to form a planar $[AgSe_3]$ unit in $AgMg_3Ga_3Se_8$, different from the six coordinated $[Li/NaSe_6]$ triangular prism units in $A^IMg_3Ga_3Se_8$ (A^I = Li, Na) and $[Ca/Sr/BaSe_6]$ triangular prism units in $A^{II}Mg_6Ga_6Se_{16}$ (A^{II} = Ca, Sr, Ba).

To evaluate the optical properties, the pure-phase powder samples of the title compounds were prepared and characterized. The experimental XRD patterns are matched well with the theoretical results derived from cif files (Fig. 3a and S3†). To obtain experimental band gaps, UV-vis-NIR diffuse reflectance spectra were measured. Based on the Kubelka–Munk function,[30–32] the experimental band gaps of $CaMg_6Ga_6Se_{16}$, $SrMg_6Ga_6Se_{16}$ and $BaMg_6Ga_6Se_{16}$ were measured to be 2.71, 2.71 and 2.69 eV, respectively (Fig. 3b). The large band gaps inherently contribute to high resistances to laser damage.[33,34] The LIDTs of the three compounds were evaluated by the single-pulse LIDT method with AGS as the reference.[35–37] The measured results show that the LIDTs of $CaMg_6Ga_6Se_{16}$, $SrMg_6Ga_6Se_{16}$ and $BaMg_6Ga_6Se_{16}$ powder samples were ∼9.0, ∼9.0, and ∼8.0 × AGS, respectively.

Beyond the band gap and LIDT, SHG response is another important parameter for IR NLO materials. The SHG responses of the title compounds were evaluated by the Kurtz and Perry method with a 2.09 μm Q-switched laser.[38–41] As shown in Fig. 3c, the SHG intensity of $CaMg_6Ga_6Se_{16}$, $SrMg_6Ga_6Se_{16}$ and $BaMg_6Ga_6Se_{16}$ was tested to be ∼1.5, ∼1.0, and ∼1.1 × AGS, respectively, showing that the A-site AEM has an influence on the SHG responses. It can be attributed to the changes of distortion degree and hyperpolarizability of nonlinear-active $[GaSe_4]$ units induced by the different A^{II}–Se chemical bonding (the bond length $d_{Ca–Se}$ = 3.0609–3.0640 Å, $d_{Sr–Se}$ = 3.1520–3.1590 Å and $d_{Ba–Se}$ = 3.2450–3.2612 Å) in the structures. Specifically, the hyperpolarizabilities of $[Ga(1–3)Se_4]$ in $CaMg_6Ga_6Se_{16}$ were calculated to 283.24, 640.08, and 665.56, while 253.14, 615.32, and 625.81 for $SrMg_6Ga_6Se_{16}$, and 190.51, 575.27, and 591.85 for $BaMg_6Ga_6Se_{16}$, thus resulting in a larger SHG response in $CaMg_6Ga_6Se_{16}$. Moreover, the hyperpolarizabilities of $[Ga(1–3)Se_4]$ in $NaMg_3Ga_3Se_8$ were calculated to be 278.91, 627.83, and 659.72, smaller than the ones in $CaMg_6Ga_6Se_{16}$. The results indicate that the alkali metal (AM) and AEM can exert an influence on the SHG response in an indirect way by modifying the geometry of NLO tetrahedral units in the $A^IB^{II}_3C^{III}_3Q^{VI}_8$ and $A^{II}B^{II}_6C^{III}_6Q^{VI}_{16}$ families. Notably, the experimental results imply that $CaMg_6Ga_6Se_{16}$ achieves a good balance between wide band gap and large SHG response, which is comparable with the recently reported typical selenide IR NLO candidates like β-$BaGa_2Se_4$ (0.6 × AGS, 2.49 eV),[25] DCL-$MgGa_2Se_4$ (0.9 × AGS, 2.96 eV),[26] $AgIn_5Se_8$ (0.7 × AGS, 1.34 eV),[42] Pb_4SeBr_6 (1.3 × AGS, 2.62 eV),[43] $KSmP_2Se_6$ (1.08 × AGS, 1.92 eV)[44] and $Na_2Ga_3In_3Se_{10}$ (1.5 × AGS, 2.47 eV)[45] (Fig. 3d).

To understand the structure–performance relationship, the band structures, total and partial density of states (TDOS/PDOS) were computed by DFT calculations.[46–48] As shown in Fig. 4a, S4a and c,† the title compounds could be direct band gap compounds with calculated GGA band gaps of 1.851 eV ($CaMg_6Ga_6Se_{16}$), 1.866 eV ($SrMg_6Ga_6Se_{16}$) and 1.853 eV ($BaMg_6Ga_6Se_{16}$). Considering the underestimation of band gaps in the standard DFT calculations with GGA because of the discontinuity of the exchange–correlation energy functional,[49,50]
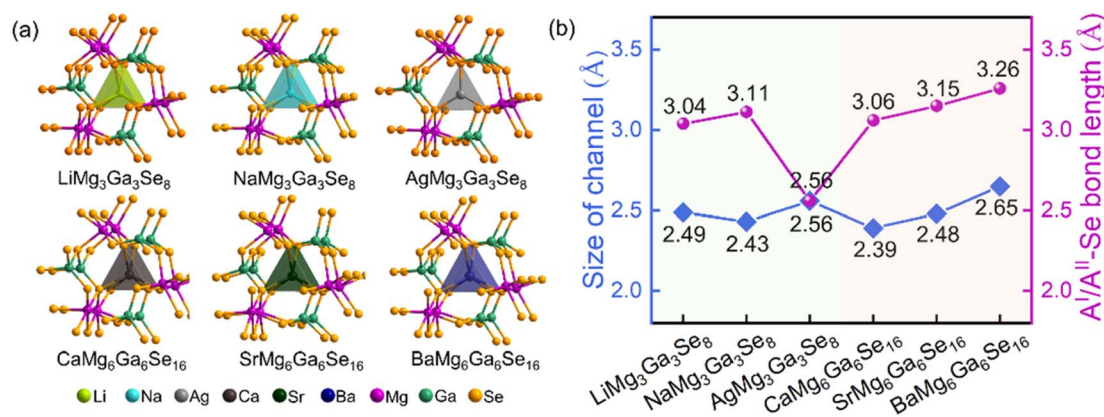

Fig. 2 (a) The atomic modes of $[Mg_3Ga_3Se_{24}]$ channels in $A^IMg_3Ga_3Se_8$ (A^I = Li, Na, Ag) and $A^{II}Mg_6Ga_6Se_{16}$ (A^{II} = Ca, Sr, Ba); (b) the statistical analyses of the channel size and A^I/A^{II}–Se band length in the six compounds.
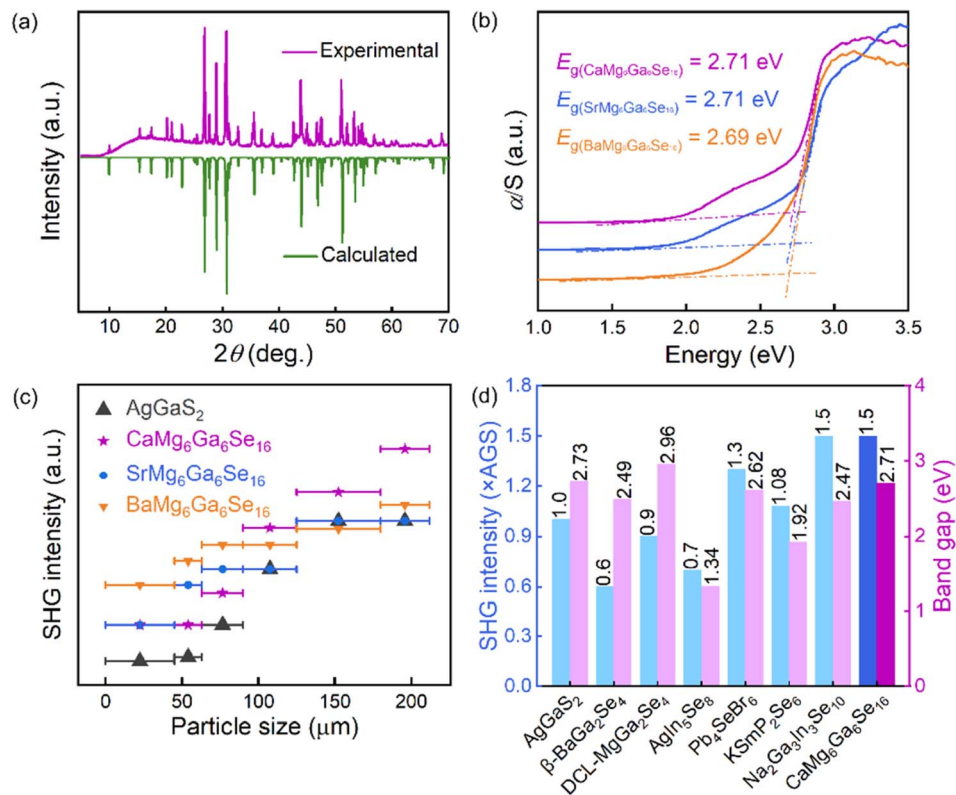
Fig. 3 (a) The XRD patterns of $CaMg_6Ga_6Se_{16}$; (b) the experimental band gaps of $A^{II}Mg_6Ga_6Se_{16}$ (A = Ca, Sr, Ba); (c) SHG intensity *vs.* AGS with similar particle sizes; (d) typical selenide IR NLO candidates with PM behaviours, AGS used as the references.

the HSE06 band gaps of the compounds were calculated to be 2.568 eV ($CaMg_6Ga_6Se_{16}$), 2.564 eV for ($SrMg_6Ga_6Se_{16}$) and 2.556 eV ($BaMg_6Ga_6Se_{16}$) (Table S14†), which are close to the experimental results in Fig. 3b. From the results of TDOS and PDOS (Fig. 4b, S4b and d†), it can be seen that the tops of the valence band maximum (VBM) near the Fermi level are
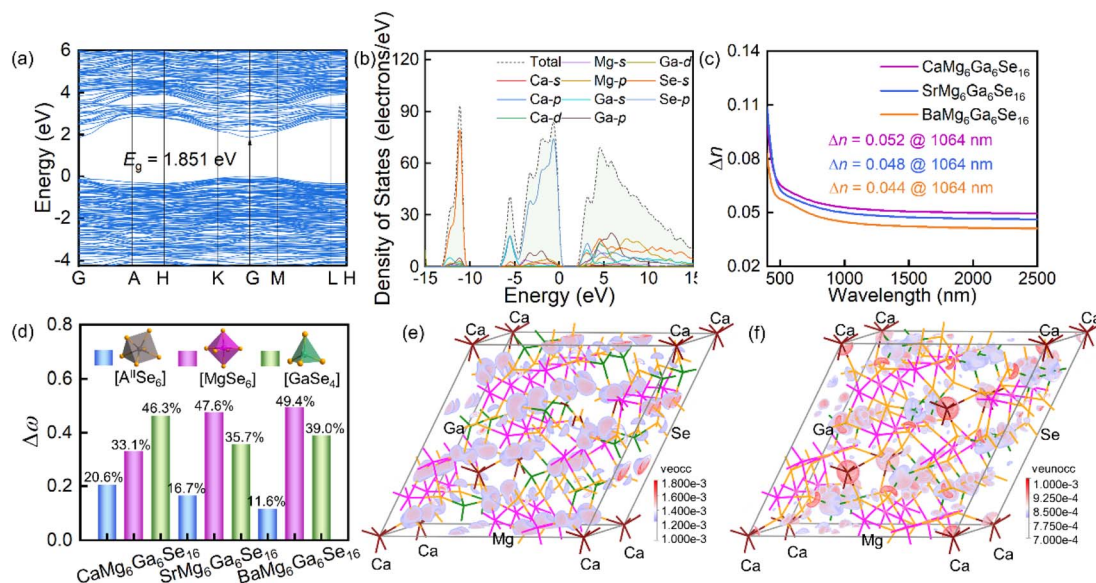

Fig. 4 (a) The band structure and (b) total and partial density of states of $CaMg_6Ga_6Se_{16}$; (c) the calculated birefringences of the title compounds; (d) the contributions ($\Delta\omega$) of $[A^{II}Se_6]$ triangular prisms, $[MgSe_6]$ octahedra and $[GaSe_4]$ tetrahedra in $A^{II}Mg_6Ga_6Se_{16}$ calculated by the response electron distribution anisotropy (REDA) method; (e and f) the SHG density maps of occupied (e) and unoccupied (f) orbitals in the VE process of $CaMg_6Ga_6Se_{16}$.

determined by Se-4p orbitals, and the bottoms of the conduction band minimum (CBM) are mainly occupied by Se-4s4p and Ga-4s orbitals, indicating that the band gaps of the three compounds are mainly determined by Ga–Se bonding in $[GaSe_4]$ tetrahedral units. Moreover, the calculated birefringence values are 0.052 for $CaMg_6Ga_6Se_{16}$, 0.048 for $SrMg_6Ga_6Se_{16}$, and 0.044 for $BaMg_6Ga_6Se_{16}$ at 1064 nm (Fig. 4c), matched with the PM behaviours in Fig. 3c. Meanwhile, the bonding electron density difference ($\Delta\rho^b$) and contributions ($\Delta\omega$) indicate that $[MgSe_6]$ and $[GaSe_4]$ units make the main contribution to the optical anisotropy in the compounds (Fig. 4d and S5†).[51]

To detect the origin of the NLO effect, the NLO coefficients and SHG density maps of the title compounds were investigated by DFT calculations.[52–56] As shown in Table S14,† the calculated NLO coefficients are $d_{11} = -11.05$ and $d_{22} = 3.92$ pm V^{-1} for $CaMg_6Ga_6Se_{16}$, $d_{11} = -10.67$ and $d_{22} = 3.93$ pm V^{-1} for $SrMg_6Ga_6Se_{16}$, $d_{11} = -10.58$ and $d_{22} = 3.71$ pm V^{-1} for $BaMg_6Ga_6Se_{16}$, which match the experimental results in Fig. 3c. Meanwhile, the SHG density maps of occupied and unoccupied orbitals in the Virtual-Electron (VE) process which occupied 93.74% in $CaMg_6Ga_6Se_{16}$, 95.25% in $SrMg_6Ga_6Se_{16}$, and 95.82% in $BaMg_6Ga_6Se_{16}$ (the Virtual-Hole (VH) process is neglected here because it accounts for a small quantity of contributions) indicate that the NLO responses of $A^{II}Mg_6Ga_6Se_{16}$ (A = Ca, Sr, Ba) also mainly originate from the $[GaSe_4]$ tetrahedral units (Fig. 4e, f and S6†), matched with the anionic group theory promoted by Chen et al.[57,58]

Conclusions

In summary, by introducing double AEM atoms into the structure, three wide band gap selenides $CaMg_6Ga_6Se_{16}$, $SrMg_6Ga_6Se_{16}$ and $BaMg_6Ga_6Se_{16}$ have been developed successfully. The compounds show strong phase-matching SHG responses (1.0–1.5 × AGS), wide band gaps (2.69–2.71 eV), high LIDTs (8.0–9.0 × AGS) and suitable birefringences (0.044–0.052 @ 1064 nm). Among them, $CaMg_6Ga_6Se_{16}$, achieving the best balance among strong SHG response (~1.5 × AGS), wide band gap (~2.71 eV) and high LIDT (~9.0 × AGS), is a promising IR NLO candidate for high power IR laser. The theoretical calculations reveal that the SHG responses and band gaps of the series of double AEM compounds originate from or are determined by the NLO-active $[GaSe_4]$ units. The results indicate that grouping 6-coordinated AEM units (triangular prisms and octahedra) and 4-coordinated NLO-active tetrahedra is a feasible way for the design of new IR NLO materials with excellent properties.

Data availability

Data available in the ESI† includes experimental sections, crystallographic data, EDS and Raman spectra, XRD patterns, band structures, the calculated bonding electron density differences and SHG density maps of the title compounds.

Author contributions

Linan Wang: investigation, methodology, writing – original draft; Dongdong Chu: DFT calculation; Zhihua Yang: software,

validation; Junjie Li and Shilie Pan: conceptualization, supervision, funding acquisition, writing – review & editing.

Conflicts of interest

There are no conflicts to declare.

Acknowledgements

Notes and references

1 Z. Y. Bai and K. M. Ok, *Coord. Chem. Rev.*, 2023, **490**, 215212.

2 H. X. Fan, N. Ye and M. Luo, *Acc. Chem. Res.*, 2023, **56**, 3099–3109.

3 Y. W. Kang and Q. Wu, *Coord. Chem. Rev.*, 2024, **498**, 215458.

4 J. J. Li and F. L. Deepak, *Chem. Rev.*, 2022, **122**, 16911–16982.

5 Y. Q. Li, J. H. Luo and S. G. Zhao, *Acc. Chem. Res.*, 2022, **55**, 3460–3469.

6 M. Mutailipu, J. Han, Z. Li, F. M. Li, J. J. Li, F. F. Zhang, X. F. Long, Z. H. Yang and S. L. Pan, *Nat. Photonics*, 2023, **17**, 694–701.

7 L. A. Wang, Q. Sun and J. J. Li, *Chin. J. Struct. Chem.*, 2023, **42**, 100013.

8 J. J. Li, J. C. Chen, H. Wang, N. Chen, Z. C. Wang, L. Guo and F. L. Deepak, *Adv. Sci.*, 2018, **5**, 1700992.

9 X. H. Dong, L. Huang, H. M. Zeng, Z. E. Lin, K. M. Ok and G. H. Zou, *Angew. Chem., Int. Ed.*, 2022, **61**, e202116790.

10 M. Mutailipu, K. R. Poeppelmeier and S. L. Pan, *Chem. Rev.*, 2021, **121**, 1130–1202.

11 X. L. Chen and K. M. Ok, *Chem. Sci.*, 2022, **13**, 3942–3956.

12 J. Chen, C. L. Hu, Y. L. Lin, Y. Chen, Q. Q. Chen and J. G. Mao, *Chem. Sci.*, 2022, **13**, 454–460.

13 J. J. Li, Z. C. Wang and F. L. Deepak, *ACS Nano*, 2017, **11**, 5590–5597.

14 G. Q. Shi, Y. Wang, F. F. Zhang, B. B. Zhang, Z. H. Yang, X. L. Hou, S. L. Pan and K. R. Poeppelmeier, *J. Am. Chem. Soc.*, 2017, **139**, 10645–10648.

15 H. N. Liu, H. P. Wu, Z. G. Hu, J. Y. Wang, Y. C. Wu and H. W. Yu, *J. Am. Chem. Soc.*, 2023, **145**, 12691–12700.

16 C. Wu, C. B. Jiang, G. F. Wei, X. X. Jiang, Z. J. Wang, Z. S. Lin, Z. P. Huang, M. G. Humphrey and C. Zhang, *J. Am. Chem. Soc.*, 2023, **145**, 3040–3046.

17 L. L. Wu, C. S. Lin, H. T. Tian, Y. Q. Zhou, H. X. Fan, S. Da Yang, N. Ye and M. Luo, *Angew. Chem., Int. Ed.*, 2023, e202315647.

18 X. F. Wang, X. D. Leng, Y. Kuk, J. Lee, Q. Jing and K. M. Ok, *Angew. Chem., Int. Ed.*, 2024, **63**, e202315434.

19 W. F. Chen, X. M. Jiang, S. M. Pei, M. S. Zhang, B. W. Liu and G. C. Guo, *Sci. China Mater.*, 2023, **66**, 740–747.

20 M. R. Sun, C. X. Li, J. L. Shi, M. H. Lee and J. Y. Yao, *Mater. Today Phys.*, 2023, **36**, 101166.

21 D. J. Mei, W. Z. Cao, N. Z. Wang, X. X. Jiang, J. Zhao, W. K. Wang, J. H. Dang, S. Y. Zhang, Y. D. Wu, P. H. Rao and Z. S. Lin, *Mater. Horiz.*, 2021, **8**, 2330–2334.

22 M. Y. Ran, A. Y. Wang, W. B. Wei, X. T. Wu, H. Lin and Q. L. Zhu, *Coord. Chem. Rev.*, 2023, **481**, 215059.

23 W. K. Wang, D. J. Mei, F. Liang, J. Zhao, Y. D. Wu and Z. S. Lin, *Coord. Chem. Rev.*, 2020, **421**, 213444.

24 J. D. Chen, H. X. Chen, F. Xu, L. L. Cao, X. T. Jiang, S. Da Yang, Y. S. Sun, X. Zhao, C. S. Lin and N. Ye, *J. Am. Chem. Soc.*, 2021, **143**, 10309–10316.

25 Y. J. Zhang, Q. Bian, H. P. Wu, H. W. Yu, Z. G. Hu, J. Y. Wang and Y. C. Wu, *Angew. Chem., Int. Ed.*, 2022, **61**, e202115374.

26 P. Wang, Y. Chu, A. Tudi, C. W. Xie, Z. H. Yang, S. L. Pan and J. J. Li, *Adv. Sci.*, 2022, **9**, 2106120.

27 A. Abudurusuli, J. B. Huang, P. Wang, Z. H. Yang, S. L. Pan and J. J. Li, *Angew. Chem., Int. Ed.*, 2021, **60**, 24131–24136.

28 J. L. Chen, Y. J. Zhang, H. P. Wu, Z. G. Hu, J. Y. Wang, Y. C. Wu and H. W. Yu, *Adv. Opt. Mater.*, 2023, **11**, 2202147.

29 L. Luo, L. A. Wang, J. B. Chen, J. Z. Zhou, Z. H. Yang, S. L. Pan and J. J. Li, *J. Am. Chem. Soc.*, 2022, **144**, 21916–21925.

30 Y. Chu, H. S. Wang, T. Abutukadi, Z. Li, M. Mutailipu, X. Su, Z. H. Yang, J. J. Li and S. L. Pan, *Small*, 2023, **19**, 2305074.

31 M. Mutailipu, M. Zhang, B. B. Zhang, L. Y. Wang, Z. H. Yang, X. Zhou and S. L. Pan, *Angew. Chem., Int. Ed.*, 2018, **57**, 6095–6099.

32 L. A. Wang, C. C. Tu, H. B. Gao, J. Z. Zhou, H. S. Wang, Z. H. Yang, S. L. Pan and J. J. Li, *Sci. China: Chem.*, 2023, **66**, 1086–1093.

33 J. Z. Zhou, K. T. Hou, Y. Chu, Z. H. Yang, J. J. Li and S. L. Pan, *Small*, 2023, DOI: **10.1002/smll.202308806**.

34 L. A. Wang, C. C. Tu, J. Z. Zhou, Y. Chu, Z. H. Yang, S. L. Pan and J. J. Li, *Adv. Opt. Mater.*, 2024, **12**, 2301634.

35 J. Z. Zhou, Z. X. Fan, K. W. Zhang, Z. H. Yang, S. L. Pan and J. J. Li, *Mater. Horiz.*, 2023, **10**, 619–624.

36 J. Z. Zhou, L. A. Wang, Y. Chu, H. S. Wang, S. L. Pan and J. J. Li, *Adv. Opt. Mater.*, 2023, **11**, 2300736.

37 J. Z. Zhou, L. Luo, Y. Chu, P. Wang, Z. Y. Guo, X. Su and J. J. Li, *J. Alloys Compd.*, 2022, **899**, 163366.

38 Y. X. Han, C. L. Hu and J. G. Mao, *Small*, 2024, **20**, 2305828.

39 W. F. Chen, B. W. Liu, S. M. Pei, X. M. Jiang and G. C. Guo, *Adv. Sci.*, 2023, **10**, 2207630.

40 X. F. Wang, Y. Wang, B. B. Zhang, F. F. Zhang, Z. H. Yang and S. L. Pan, *Angew. Chem., Int. Ed.*, 2017, **56**, 14119–14123.

41 H. S. Wang, Y. Chu, X. T. Pan, Z. H. Yang, S. L. Pan and J. J. Li, *Mater. Today Phys.*, 2023, **38**, 101243.

42 L. F. Dong, S. Z. Zhang, P. F. Gong, F. Liang and Z. S. Lin, *Inorg. Chem. Front.*, 2023, **10**, 3248–3254.

43 J. K. Wang, H. P. Wu, H. W. Yu, Z. G. Hu, J. Y. Wang and Y. C. Wu, *Adv. Opt. Mater.*, 2022, **10**, 2102673.

44 Z. X. Chen, C. Y. Zhao, X. H. Li, W. D. Yao, W. L. Liu and S. P. Guo, *Small*, 2023, **19**, 2206910.

45 J. Li, W. D. Yao, J. N. Li, X. H. Li, W. L. Liu and S. P. Guo, *Mater. Today Phys.*, 2023, **32**, 101007.

46 J. J. Li, Z. Lian, Q. Li, Z. C. Wang, L. F. Liu, F. L. Deepak, Y. P. Liu, B. Li, J. Y. Xu and Z. X. Chen, *Nano Res.*, 2022, **15**, 5933–5939.

47 Y. Wang, B. B. Zhang, Z. H. Yang and S. L. Pan, *Angew. Chem., Int. Ed.*, 2018, **57**, 2150–2154.

48 M. Yan, R. L. Tang, W. D. Yao, W. L. Liu and S. P. Guo, *Chem. Sci.*, 2024, **15**, 2883–2888.

49 H. S. Wang, X. T. Pan, W. Zhao, Y. Chu and J. J. Li, *Inorg. Chem. Front.*, 2023, **10**, 6253–6261.

50 B. B. Zhang, G. Q. Shi, Z. H. Yang, F. F. Zhang and S. L. Pan, *Angew. Chem., Int. Ed.*, 2017, **56**, 3916–3919.

51 B. H. Lei, Z. H. Yang, H. W. Yu, C. Cao, Z. Li, C. Hu, K. R. Poeppelmeier and S. L. Pan, *J. Am. Chem. Soc.*, 2018, **140**, 10726–10733.

52 Y. Chu, H. S. Wang, Q. Chen, X. Su, Z. X. Chen, Z. H. Yang, J. J. Li and S. L. Pan, *Adv. Funct. Mater.*, 2023, DOI: **10.1002/adfm.202314933**.

53 Y. Chu, P. Wang, H. Zeng, S. C. Cheng, X. Su, Z. H. Yang, J. J. Li and S. L. Pan, *Chem. Mater.*, 2021, **33**, 6514–6521.

54 L. A. Wang, D. D. Chu, D. Q. Yin, C. W. Xie, Z. H. Yang, J. J. Li and S. L. Pan, *Mater. Today Phys.*, 2023, **38**, 101245.

55 X. F. Wang, J. J. Li, Z. J. Zhao, S. M. Huang and W. H. Xie, *J. Appl. Phys.*, 2012, **112**, 023701.

56 M. Y. Zhang, N. W. Liang, D. Hao, Z. X. Chen, F. Zhang, J. Yin, Y. H. Yang and L. S. Yang, *Nano Research Energy*, 2023, **2**, e9120077.

57 C. T. Chen, *Acta Phys. Sin.*, 1977, **26**, 486–499.

58 H. T. Qiu, F. M. Li, C. C. Jin, Z. H. Yang, J. J. Li, S. L. Pan and M. Mutailipu, *Angew. Chem., Int. Ed.*, 2024, **63**, e202316194.